1 KSME Journal, Vol. 7, No. 1, pp. 1~13, 1993

A Numerical Study of Three-Dimensional Backward-Facing Step Flow

S.O. Park*, K.S. Lim and R.H. Pletcher*****

(*Received June 15, 1992*)

The laminar and turbulent flow over a backward-facing step placed in a square duct was investigated numerically. The aspect ratio of the step (step width/step height) was 3 and the area expansion ratio was 2 : 3. Three-dimensional effects were significant due to the small aspect ratio. To simulate turbulent flows, both a standard k-ε model and a non-linear k-ε model were employed and the results were compared. The non-linear model was found to yield better results. From the numerical results, the existence of the corner vortex and the flow field associated with it were clarified. The reattachment length of the three-dimensional flow was found to be considerably shorter than the corresponding two-dimensional flow. The evolution of longitudinal vortices was visualized. Surface flow patterns which clearly demonstrate three-dimensional aspects of the flow were presented. Based on various data available, topological flow pattern was also sketched. To support the findings explored in the present work, experimental data were compared with the numerical data where applicalble.

Key Words: Backward-Facing Step Flow, Three-Dimensional Turbulent Flow, Aspect Ratio, Non-Linear Turbulence Model, Corner Vortices, SIMPLE-C

Nomenclature

$A_E, A_W, A_N, A_S, A_T, A_B$: Finite-difference coefficients
$C_1, C_2, C_\mu, C_D, C_E$: Turbulence model constants
G : Production rate of k
h : Step height
k : Turbulent kinetic energy
P : Static pressure
Re : Reynolds number based on step height$\left(=\frac{Uoh}{v}\right)$
S^ϕ : Integrated source term in finite difference equation
U, V, W : Local velocity in each direction
$\vec{U}$: Velocity vector
Uo : Reference velocity in the plane of the step edge
$\overline{u}'$, $\overline{v}'$: r.m.s. value of velocity fluctuations
x, y, z : Longitudinal, Transverse, Spanwise Coordinates
x_r : Reattachment length

Greek Symbols

Γ : Diffusion coeffieient
ε : Dissipation rate of k
μ : Molecular viscosity
μ_t : Turbulent viscosity
$\sigma_k, \sigma_\varepsilon$: Turbulence model constants
ϕ : Scalar quantity
ρ : Fluid density
τ_{ij} : Reynolds stress tensor

* Department of Aerospace Engineering, Korea Advanced Institute of Science and Technology, Kusong-Dong 373-1, Yusung-Ku, Taejon, Korea
** Senior Research Scientist, Chinhae Research Laboratory, Agency for Defense Development
*** Department of Mechanical Engineering, Iowa State University, Ames, Ia, U.S.A.

τ_w : Wall shear stress

Abbreviations

F : Foci at the surface
N : Nodal point
S : Saddle point

1. Introduction

Numerical and experimental studies of the two-dimensional backward-facing step flow have been reported by many authors. However, three-dimensional backward-facing step flow has not received much attention to date ; reported works on the three-dimensional flow are rare. Three-dimensional backward-facing step flow is quite complex in nature in spite of its simple geometry. The flow geometry considered in this study is essentially identical to that of two-dimensional backward-facing step flow except for the fact that the aspect ration is very small. Here, the aspect ratio is defined as the ratio of the width to the height of the backward-facing step. Thus, in a low aspect ratio backward-facing step flow (referred to as three-dimensional backward-facing step flow hereinafter), the effect of sidewalls confining the step will be significant. The three-dimensionality of the flow is mainly due to the secondary motion, which can arise from two different sources; one is pressure driven, and the other turbulent stress driven (Bradshaw, 1987). Obviously, the secondary motion can greatly alter the flow characteristics. So far, many research efforts on the flow have been directed toward the study of corner flows (Bradshaw, 1987 ; Gessner, 1982) or of flows through a bend (Humphrey et al., 1981). Further, most of the studies were limited to parabolic flows in which downstream influences on the flow were negligible. Since a backward-facing step flow involves a large separated zone, the flow is elliptic in nature. Also, owing to the abrupt area change in the plane of step face, it is expected that the major secondary motion will be the pressure-induced one. However, far downstream of the step, this motion will be gradually relaxed to the turbulence-driven one. An adequate simulation of transition from the pressure-induced secondary motion to turbulence-driven one may be a good test problem for any turbulence model to be used in three-dimensional flows.

It was found experimentally by de Brederode and Bradshaw(1972) that three-dimensional effects become important in backward-facing step flows if the aspect ratio is less than 10. As a model for the present study, we selected the backward-facing step flow which undergoes two to three expansion, and of which the aspect ratio (of the step) is 3. The cross-section downstream of the step face, therefore, is square ; turbulence-driven secondary motion in a duct of constant cross-section is well documented (Demuren and Rodi, 1984). The primary objective of this investigation, as an extension of our earlier work (Lim et al., 1990), is to increase our understanding of complex three-dimensional turbulent flow field of a backward-facing step. Though simple in geometry, understanding of such a flow is important in practice, for it represents a basic flow configuration for various bluff-body flows such as encountered in combustors, the flow around buildings, and around protuberances in a flow passage. An adequate numerical simulation of a three-dimensional backward-facing step flow will shed light on the physics of the flow which is not yet clearly understood.

In the present study, the flow field was computed under both laminar and turbulent conditions. Since the laminar flow (numerical) simulation requires no assumptions about turbulence modeling, the laminar flow solution was often compared qualitatively with the turbulent solution to elucidate the turbulent flow field. This was felt necessary simply because of lack of reliable experimental data. The numerical scheme employed to solve the present problem (three-dimensional incompressible Naiver-Stokes equations) is based on the finite volume formulation and SIMPLE-C (Van Doormal and Raithby, 1984).

The emphasis was on turbulent flow in this

study. It was felt necessary to use a turbulence model capable of capturing turbulence-driven secondary flow for the present problem. We selected the non-linear two-equation model proposed by Speziale(1987). It was shown by Speziale that the model successfully produced secondary motion in a fully developed square duct flow. An algebraic stress model is also known to be capable of producing anisotropic turbulent stresses. However, in the present study, the non-linear k-ε model was adopted because it was simpler to use than the algebraic stress model.

Flow patterns of secondary motion at several downstream cross-sections were given to clarify the three-dimensional nature of the flow. Surface flow patterns and fluid particle paths were added to increase our understanding of the flow. The evolution and decay of corner vortices, which seems to be essential in describing three-dimensional sidewall effect, was explained.

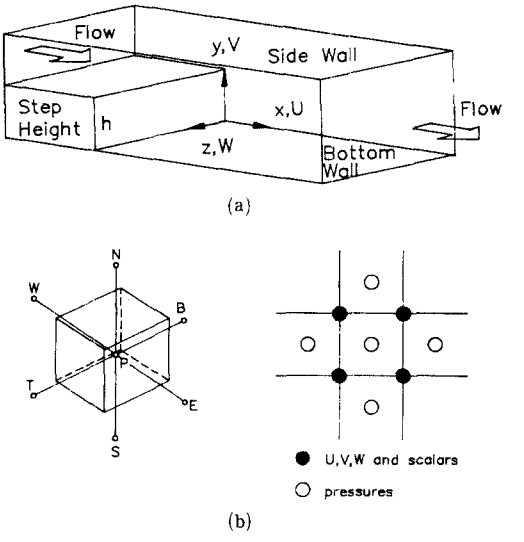

Fig. 1 (a) The flow configuration and the coordinate system
(b) Control volume representation

2. Mathematical Model

The flow configuration with the coordinate system for the present work is depicted in Fig. 1(a). The flow was assumed to be steady and incompressible.

The continuity and the time-averaged Navier-Stokes equations are written in Cartesian tensor form as:

$$(\partial/\partial x_j)(\rho U_j)=0.0, \tag{1}$$

$$(\partial/\partial x_j)(\rho U_i U_j)=-\partial p/\partial x_i+(\partial/\partial x_j)[\mu(\partial U_j/\partial x_i+\partial U_i/\partial x_j)-\overline{\rho u_i' u_j'}], \quad (i,j=1,2,3) \tag{2}$$

The Reynolds stresses in Eq. (2) are modeled by a two-equation turbulence model. The conventional set of k-ε model equations (Launder and Spalding, 1974) is given as:

$$(\partial/\partial x_j)(\rho U_j k)=(\partial/\partial x_j)\left[\frac{\mu_t}{\sigma_k}(\partial k/\partial x_j)\right]+\rho G-\rho\varepsilon, \tag{3}$$

$$(\partial/\partial x_j)(\rho U_j \varepsilon)=(\partial/\partial x_j)\left[\frac{\mu_t}{\sigma_\varepsilon}(\partial \varepsilon/\partial x_j)\right]+\rho\frac{\varepsilon}{k}[C_1 G-C_2\varepsilon], \tag{4}$$

$$-\overline{\rho u_i' u_j'}=-\frac{2}{3}\rho k\delta_{ij}+\mu_t(\partial U_j/\partial x_i+\partial U_i/\partial x_j), \tag{5}$$

$$\mu_t=\rho(C_\mu k^2/\varepsilon), \tag{6}$$

$$G=-\overline{u_i' u_j'}(\partial U_i/\partial x_j), \tag{7}$$

$$C_1=1.44,\ C_2=1.92,\ C_\mu=0.09,\ \sigma_k=1.0,\ \sigma_\varepsilon=1.3. \tag{8}$$

The standard set of k-ε model equations is not capable of producing anisotropic normal stresses as can be clearly seen from Eq.(5). In the model proposed by Speziale(1987) which can produce anisotropic normal stresses to make it possible to predict turbulence-driven secondary flows, the constitutive relation (Eq.(5)) and the production term (Eq.(3)) are modified as follows while the transport ransport equations remain the same.

$$\tau_{ij}=-\overline{\rho u_i' u_j'}=-\frac{2}{3}\rho k\delta_{ij}+2\mu_t\bar{D}_{ij}+\frac{4}{3}\rho C_\mu^2(k^3/\varepsilon^2)[C_D(\bar{D}_{im}\bar{D}_{mj}-\bar{D}_{mn}\bar{D}_{mn}\delta_{ij})+C_E(\dot{\bar{D}}_{ij}-\dot{\bar{D}}_{mn}\delta_{ij})], \tag{9}$$

$$G=-\overline{\rho u_i' u_j'}(\partial U_i/\partial x_j)=\nu_t(\partial U_j/\partial x_i+\partial U_i/\partial x_j)(\partial U_i/\partial x_j)+4/3C_\mu^2 k^3/\varepsilon^2$$

$$[C_D(\bar{D}_{im}\bar{D}_{mj}-\bar{D}_{mn}\bar{D}_{mn}\delta_{ij})+4/3C_E (\dot{\bar{D}}_{ij}-\dot{\bar{D}}_{mm}\delta_{ij}/3)](\partial U_i/\partial x_j), \quad (10)$$

$$\bar{D}_{ij}=\frac{1}{2}(\partial U_j/\partial x_i+\partial U_i/\partial x_j), \quad (11)$$

$$\dot{\bar{D}}_{ij}=U_n(\partial/\partial x_n)\bar{D}_{ij}-(\partial U_i/\partial x_n)\bar{D}_{nj} -(\partial U_j/\partial x_n)\bar{D}_{ni}, \quad (i, j, m, n=1,2,3) \quad (12)$$

$$C_D=1.68, \quad C_E=1.68. \quad (13)$$

As can be seen from Eqs. (9) and (10), the non-linear model differs from the standard one by the addition of the last two terms, which might be called the non-linear terms.

3. Numerical Procedure

3.1 Finite volume equations and grid system

To solve the present problem, Chen's CNS3D code(1986) based on the SIMPLE-C algorithm (Van Doormal and Raithby, 1984) was adopted and modified. The main modifications involved the turbulence model. Amano's scheme(1984) for the discretization of the convective and diffusive flux terms were also implemented. Amano used a fourth-order expansion of the exponential term of the Spalding's(1972) exponential scheme to make improvements over the conventional hybrid-scheme. The numerical solution procedure combines finite volume integration techniques for the momentum and scalar transport equations and pressure correction equation to enforce local and global mass conservation. The discretized equations are obtained by casting the governing equations into a generic transport equation and then integrating the generic equation over the control volume shown in Fig. 1(b). The resulting discretized representation for the general transport equation can be expressed as

$$A_P\phi_P=A_E\phi_E+A_W\phi_W+A_N\phi_N+A_S\phi_S +A_D\phi_D+A_U\phi_U+S^\phi\delta(Vol). \quad (14)$$

Where the link coefficients A_E, A_W, $\cdots$, involve convection, diffusion, and area terms. S^ϕ is the source term. For the details of the derivation, the readers are refered to Patankar(1980) and Chen (1986). Equation (14) is solved using one sweep of a tridiagonal matrix solver in each direction. For computation with the non-linear k-ε model, the non-linear terms of Eq. (9) were included in the source term.

A staggered grid system where all the velocity components are at the grid nodes and the pressure is assigned at the corners of the velocity control volume was employed (Fig. 1(b)). A conventional staggered grid system often requires modification of link coefficients in Eq. (9) for the velocity points adjacent to the obstruction, since the contributions to the coefficients owing to the blocked control volume by the obstacle should be accounted for. Durst and Rastogi(1979) observed that their calculations using a conventional grid system produced unrealistic results in the region downstream of the obstruction if proper modification was not made. However, the present grid system does not require any modifications to the coefficients.

A three-dimensional mesh of grid lines in the x, y, and z directions was constructed throughout the computational domain using a stretching transformation such that the grid lines were concentrated near the step edge (Fig. 2(a)). The computational domain consists of the half of the flow domain divided by the centerplane of the symmetry. For turbulent flow, preliminary numerical experiments revealed that the convergence was strongly influenced by the grid distribution near the step. It was also realized that the present numerical solution was particularly sensitive to

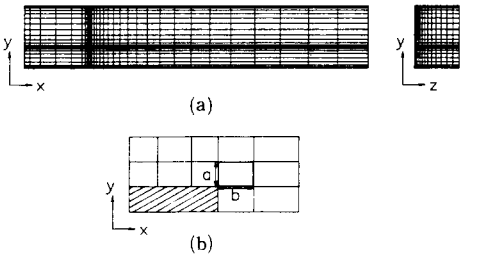

(a) The complete grid distribution
(b) A typical mesh near the step

Fig. 2 Typical grid arrangement

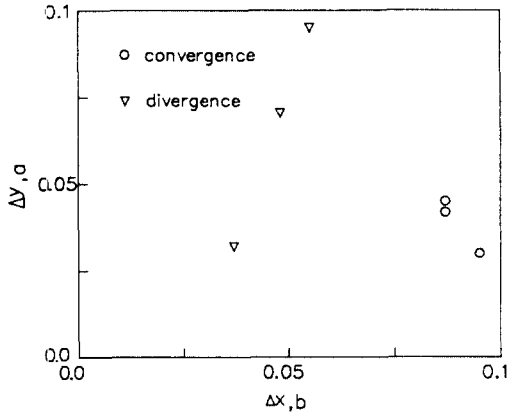

Fig. 3 Convergence dependency on the grid refinement

the aspect ration (ratio of a/b in Fig. 2(b)) of the computational cell near the salient edge of the step. Figure 3 shows various grid aspect ratios at which converged solutions were obtained. As can be seen, the convergence depended strongly on the aspect ratio of the cell. A converged solution was obtained when $b<a$. A plausible explanation for this can be given as follows. For the purpose of illustration, consider the pressure-correction equation in two-dimensional flow which can be written as

$$A_P P'_P = A_E P'_E + A_W P'_W + A_N P'_N + A_S P'_S + S^P, \tag{15}$$

where

$$S^P = \{(\rho U^*)_w - (\rho U^*)_e\} a + \{(\rho V^*)_s - (\rho V^*)_n\} b. \tag{16}$$

We note here that the source term S^P is another form of mass conservation principle. Near the edge of the step, it is likely that the $\partial U/\partial y$ term is considerably larger than the $\partial V/\partial x$ term. Therefore, to closely approximate the mass conservation term, a very small 'a'(that is Δy) would be necessary. If the grid spacing, 'a' were large, the mass conservation may not be represented correctly which may cause divergence of the solution. The converged solution was not influenced significantly by the spanwise grid spacing in the shear layer as long as the grid is clustered near the side wall.

For laminar flow computations, a $36\times31\times21$ (x^*y^*z) grid was used. The computaional domain ranged from $x/h=0.0$ (the plane of the step) to $x/h=20$. The laminar flow computation was of a somewhat preliminary nature and was carried out to evaluate the convergence of the solution algorithm. Computations were carried out for the case of the Reynolds number of 100, 300, and 500. The Reynolds number was based on the average inlet velocity and the step height. For turbulent flow computations, a $32\times22\times15$ (x^*y^*z) grid was used. The computational domain ranged from $x/h=-4$ (upstream of the step face) to $x/h=20$. A rigorous grid dependence test was not carried out. However, computations using a coarser grid ($21\times21\times15$) resulted in a flow field very close to the one obtained with the $32\times22\times15$ grid. The differences in the mean velocity profiles between two grid systems were at most 1%. From this, it was decided that the $32\times22\times15$ grid system might be sufficient for the purpose of present study. Three Reynolds numbers were considered : 1.0×10^4, 7.0×10^4 and 1.0×10^5.

The solutions were considered to be converged when the following convergence criterion was met.

$$(|\Delta U|_{max}+|\Delta V|_{max}+|\Delta W|_{max})/U_{ref}+|\Delta P|_{max}/U_{ref}^2 \le 1.0\times10^{-4}, \tag{17}$$

where U_{ref} is the average inlet velocity. About 1000~1200 iterations were necessary for convergence when the standard k-ε model used. When the non-linear k-ε model was used, additional 700~800 iterations were necessary. In this case, the converged solution field with the standard k-ε model was taken as the initial data.

3.2 Boundary conditions

Turbulent flow ; On the downstream boundary plane, the Neumann boundary condition, $\partial\phi/\partial x=0$, where ϕ denotes any physical variable, was prescribed. Near the wall, standard wall functions (Launder and Spalding, 1974) were applied to save grid points in the near wall region. The following functions were used.

$$\left(\frac{\tau}{\rho}\right)_w = k\vec{U}_p C_\mu^{1/4} k_p^{1/2} / ln(Ey_p C_\mu^{1/4} k_p^{1/2}/\nu), \tag{18}$$

$$\varepsilon_p = C_\mu^{3/4} K_p^{2/3}/(xy_p), \tag{19}$$

$$K_p = \left(\frac{\tau}{\rho}\right)_w C_\mu^{1/2}. \tag{20}$$

The subscript 'p' refers to the grid point next to the wall and $\vec{U}_p$ represents velocity vector parallel to the wall. At the inlet, a uniform distribution of all variables was prescribed and the secondary velocities were set to zero. The turbulent kinetic energy, k, and its dissipation rate, ε, were given as follows (Qin, 1984).

$$k_{in} = 0.003 \times U_{in}^2,$$
$$\varepsilon_{in} = 0.09 \times k_{in}^{1.5}/(0.03 \times h), \tag{21}$$

where the subscript 'in' refers to the inlet plane. The above boundary condition is the one typically employed in predictions when no experimental boundary condition is available (Nallasamy, 1985).

At the symmetry plane, the velocity, W, was set to zero, while all the other quantities were required to have zero gradient normal to this plane.

Laminar flow; At the wall boundary, no slip conditions were specified. At the face of inflow boundary of the plane of the step edge, fully developed velocity profile was prescribed, the analytic form of which is readily available (White, 1974). Boundary conditions for outflow plane and symmetry plane were given the same manner in the turbulent flow computations.

4. Results and Discussion

4.1 Laminar flow

Figure 4 compares the predicted reattachment length in the centerplane with those of two-dimensional results (Denham and Patrik, 1974; Hackman et al., 1984) for the Reynolds number range of 0~500. As can be seen, the present computation successfully reproduced the tendency that the reattachment length increases with the Reynolds number. One may also note that the reattachment length in three-dimensional flow is slightly shorter than in two-dimensional flow.

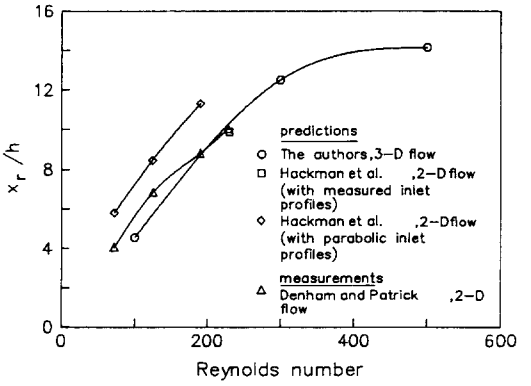

Fig. 4 Reattachment length versus Reynolds number for laminar flow

Cross-sectional velocities at several downstream stations are vector-plotted in Fig. 5. It is interesting to observe the development of secondary motion with downstream distance. Clearly, the velocity vectors depicted in Fig. 5(a) show that the major secondary motion outside of the recirculation zone is in the downward direction, which can be anticipated since the cross-sectional area for the streamwise mass flow is expanding. As the flow proceeds further out of the recirculation zone, the downward motion is developed to form a pair of horseshoe-like streamwise vortices (what we see in Fig. 5(c) is one of the pair).

Since the laminar flow in straight constant area square duct will eventually be fully developed with zero cross-sectional velocities, the secondary motion seen in Fig. 5 is expected to die out far downstream. The length of the duct necessary for the flow to adjust to a (new) fully developed state will be quite long, since the time scale for the secondary motion to decay will be governed by the molecular viscosity. Figure 6 shows the surface flow pattern in laminar flow. The spanwise location of the line of separation clearly indicates that the flow is strongly three-dimensional and the reattachment length of the recirculating region varies across the duct width. A node can be identified in the surface flow pattern of the bottom wall. It is also noted that the reattachment

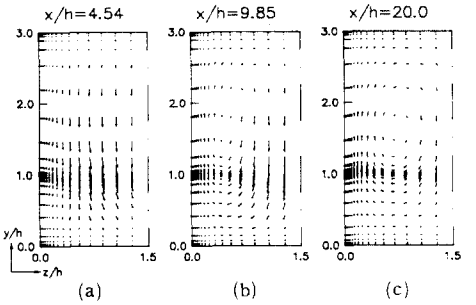

Fig. 5 Cross-sectional velocity in laminar flow ($Re=1.0\times10^2$)

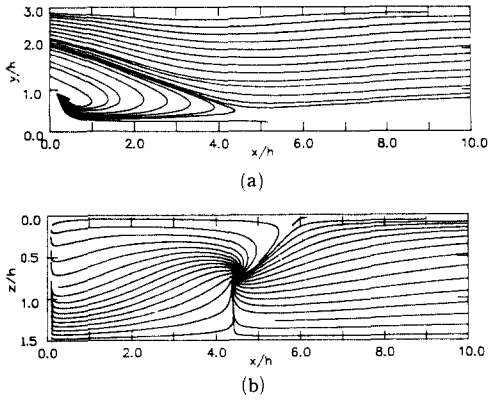

(a) Sidewall
(b) Bottom wall

Fig. 6 Surface flow patterns in laminar flow ($Re=1.0\times10^2$)

line is bulged outward. The bulging phenomena near the side wall was experimentally observed in Armaly et al.'s work(1983).

4.2 Turbulent flow

As mentioned previously, a standard k-ε turbulence model and a non-linear k-ε model were employed for the present simulation. The non-linear k-ε model was felt to be necessary if we were to take due account of the turbulence driven secondary motion, which is well known to be present in straight duct of any non-circular cross-section. It should be mentioned here that numerical difficulties were encountered when the non-linear k-ε model was used. The use of non-linear model from the start of the calculation was unsuccessful. Therefore, in the initial stage of iteration, the calculations were carried out using the standard model. After several iterations, the turbulence model was then switched to the non-linear one. The other numerical problem encountered was one associated with the first grid points near the wall boundary. The non-linear term of Eq. (9) became abnormally large at those points. Thus, it was necessary to omit the non-linear term at the first (from the wall) grid points. This procedure is equivalent to the omitting the source terms producing the secondary motion at the first grid points (Rodi, 1982) when the algebraic stress model is used.

Streamwise mean velocity profiles in the centerplane ($z/h=1.5$) and in the quarterplane ($z/h=0.5$) of the three-dimensional backward-facing step flow of the aspect ratio 3 and the area expansion ratio 2:3 are displayed in Fig. 7(a). The Reynolds number based on the step height is 7.0×10^4. The predictions using the non-linear turbulence model and those using the standard model differ little from each other. The standard model predicts slightly larger velocities in the shear layer. The turbulent kinetic energy profiles depicted in Fig. 7(b) show larger disagreements between the two predictions. The non-linear model gives a larger peak value of the kinetic energy in the shear layer. Also, the transverse location of the peak value is higher in the predictions using the non-linear model. Eaton(1980) found that when the peak value was larger and the transverse location was higher, the reattachment length became longer. The ability of the non-linear model to predict higher peak values of the kinetic energy seem to render the reattachment length longer, as was demonstrated by Speziale (1987) for two-dimensional flows. However, in the three-dimensional case, the reattachment length predicted using the non-linear model did not differ greatly from the one with the standard model. We attribute this fact to the effect of secondary motion.

Both the non-linear model and the standard one predicted the reattachment length to be about

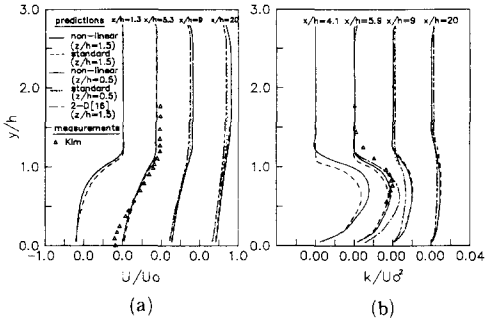

(a) Velocity profiles
(b) Turbulent kinetic energy profiles

Fig. 7 Selected longitudinal profiles in the duct flow for the aspect ratio of 3.0 and area expansion ratio of 2:3 ($Re = 7.0 \times 10^4$)

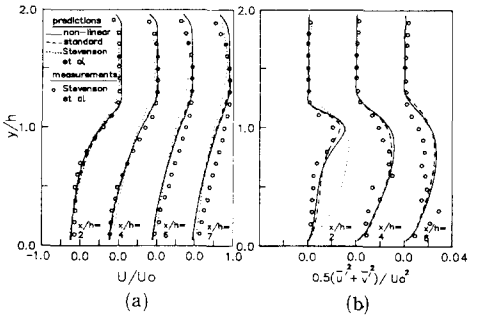

(a) Velocity profiles
(b) Turbulent kinetic energy profiles

Fig. 8 Selected longitudinal profiles in the duct flow for the aspect ratio of 1.0 and area expansion ratio of 1:2 ($Re = 1.75 \times 10^5$)

5.0～5.3 times the step height in the centerplane. The non-linear model produced a slightly longer reattachment length. In two-dimensional flow, the non-linear model resulted in a significant increase in reattachment length over the standard model (Speziale, 1987). The reattachment length in two-dimensional flow with the same expansion ratio is about 6.0～7.0 times the step-height (Eaton and Johnston, 1981 ; Kim, 1987). Thus, it can be said that the reattachment length is much shorter in three-dimensional case than in the corresponding two-dimensional case. In three-dimensional flow, the secondary motion enhances momentum exchange between the mainstream and the recirculation zone. As a result, the strength of recirculation is weakened, and hence the reattachment length shortens.

To support these findings, we calculated a three-dimensional backward-facing step flow of aspect ratio of 1.0 and area expansion ration of 1: 2, for which some experimental data was available in Stevenson et al.'s(1984) work. As can be seen from Fig. 8, the prediction of mean velocities, turbulent kinetic energy, and reattachment length agree well with the experimental data. The mean velocity and kinetic energy profile comparions with the experimental data in Fig. 8 clearly show that the results of the three-dimensional calculations give much better agreement to the experimental data than the Stevenson et al.'s two-dimensional predictions. The present numerical calculation predicted the reattachment length to be about 7. It should be noted here that Stevenson et al. predicted the reattachment length to be about 7 times the step height (for agreement with experimental measurement) by modifying the model constant of the dissipation rate equation. They performed purely two-dimensional calculation. At a first glance, our computational results about the reattachment length for this case seem contradictory to the finding that the reattachment length was about 5.0～5.3 times the step height for the flows of the aspect ratio of 3. It is natural that we should expect shorter reattachment length when the aspect ratio is 1. However, the Stevenson et al.'s result showed that it was even longer. To clarify this anomaly, we performed several calculations for the Stevenson et al.'s geometry for various Reynolds numbers. The results are illustrated in Fig. 9. As can be seen, the effect of the Reynolds number is very significant for this case. Stevenson et al.'s experiment corresponds to the Reynolds number of 1.75×10^5. The results shown in Fig. 9 point out that the reattachment length is about 5.4 when the Reynolds number is 1.0×10^4. Thus, our conclusion that reattachment length in the three-dimensional flow is shorter than in two-dimensional one is not obscured by the

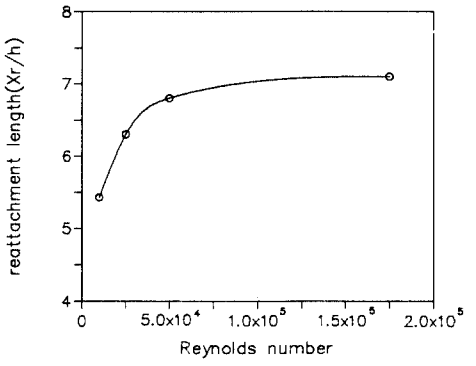

Fig. 9 Predicted reattachment length as function of Reynolds number in the turbulent flow

Stevenson et al.'s experimental results. When the aspect ratio was 3, the reattachment length in the centerplane varied little with the Reynolds number in the present range of numerical experiment (However, the location of corner vortices changed sensitively with the Reynolds number as discussed later). A very analogous phenomenon in which the Reynolds number effect becomes important as aspect ratio decreases can be found in Couette flow between rotating concentic cylinders. In this cose, a critical Reyndds number at which wavy vortex flow develops is strongly dependent on height-to-width ratio (Di Prima and Stuart, 1983).

To take a look at cross-sectional flow patterns, we now return to the case of our major effort, that is, the case of three-dimensional backward-facing step flow of aspect ratio 3 and area expansion ratio 2:3. Fig. 10(a) and 10(b) illustrates, respectively, the cross-sectional flow velocities obtained with the standard k-ε model and the non-linear k-ε model. Both figures show the evolution of longitudinal vortices. However, the detailed vortical flow patterns are considerably different from each other. The center of the primary vortex at $x/h=20$ in Fig. 10(a) is located higher than the one in Fig. 10(b). Further, at $x/h=5$ and 9 in Fig. 10(b), the formation of weaker vortices are clearly visible near the bottom corners, while it is not so in Fig. 10(a). The qualitative behavior of longitudinal vortex development observed in the results

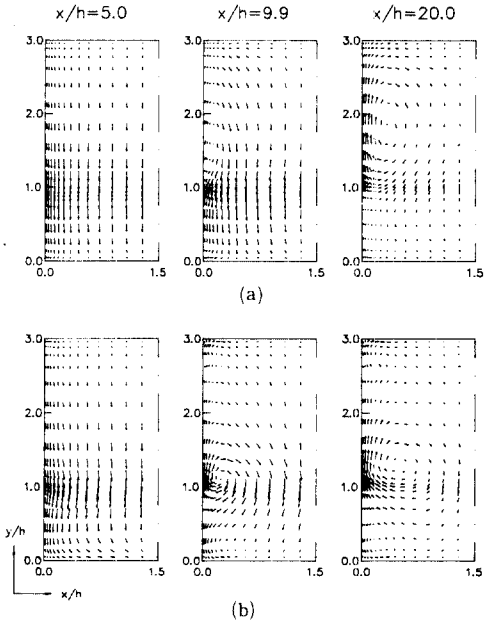

(a) The prediction with standard k-ε model
(b) The prediction with non-linear k-ε model

Fig. 10 Cross-sectional velocity in the turbulent flow ($Re=7.0\times10^4$)

obtained with the standard model (Fig. 10(a)) is somewhat similar to that of laminar flow (Fig. 5). It is notable that the center of the primary vortex in turbulent flow of Fig. 10 (a) is located at about the same height of the one in laminar flow (Fig. 5). But, it is noted that the center of the primary vortex predicted with the non-linear (Fig. 10(b)) is considerably lower than the one with the standard model (Fig. 10(a)). The discrepancy between the location of the vortex center, however, did not affect mean velocity and kinetic energy profiles significantly. This can be ascertained in Fig. 7(a) and 7(b). The mean velocity and turbulent kinetic energy profile predictions using different turbulence model differ little from each other. Considering the fact that the standard model is not capable of producing turbulence-driven secondary motion, the main thrust for the cross-sectional flow must be pressure-driven. In fact, the curved flow passage caused by the blockage effect can be considered as the major source of secon-

dary motion. When the flow starts to adjust to the constant cross-sectional area outside of the recirculation zone, we expect that the flow experiences differences in normal stresses. Since the standard k-ε model is not capable of generating anisotropy property in normal stresses, the turbulence-driven secondary motion is not effected adequately. Perhaps, this can explain the qualitative resemblance between cross-sectional velocity patterns in laminar flow (Fig. 5) and those in trubulent flow with the standard model (Fig. 10(a)). We may conclude that the discrepancy between Fig. 10(a) and Fig. 10(b) is due to the effect of turbulence-driven secondary flow. Obviously, the anisotropy in turbulence is seen to play a considerable role in establishing secondary motion far outside of the recirculation region as seen in Fig. 10(b).

The surface flow patterns on the bottom and on the side wall obtained from the numerical results are displayed in Fig. 5 (laminar flow) and Fig. 11 (turbulent flow). Also, the tracks of particles departed from the bottom wall just downstream and just upstream of the step face in the turbulent flow are shown in Fig. 12. It is seen that a fluid particle from the boundary layer around the corner between the duct sidewall and the (upper) bottom floor of the step enters the separated region, recirculates in a spiral fashion toward the centerplane and leaves the separated region near the reattachment line (Fig. 12(a)). Flow particles leaving bottom floor is seen to spiral toward the corner between the bottom wall and the sidewall. Three-dimensional particle motion exhibited in Fig. 12(a) is very similar to the one illustrated by Goldstein et al.(1970).

Based on the surface flow patterns, particle paths, and velocity data, we were able to sketch the topological features of the present flow, which is depicted in Fig. 13. The position and shape of the corner vortices (represented as two foci) are very similar to those depicted by Ruderich and Fernholz(1986). It is notable that all the limiting streamlines on the bottom wall are connected to the corner vortex (Fig. 11 and Fig. 13). This

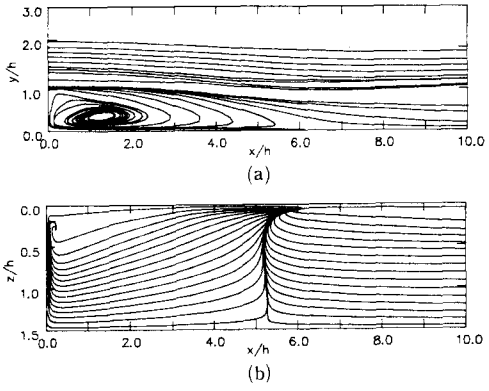

(a) Sidewall (b) Bottom wall

Fig. 11 Suface flow patterns predicted with nonlinear k-ε model ($Re=7.0\times10^4$)

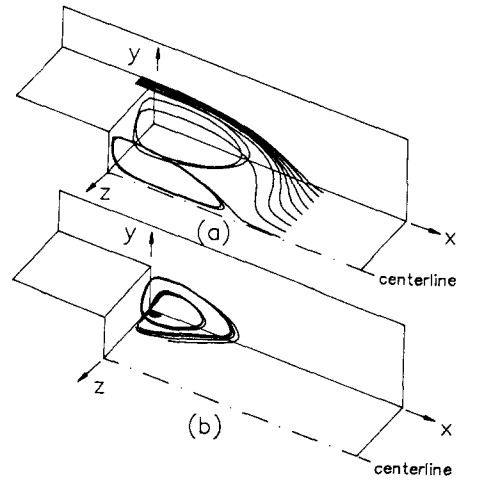

(a) Particle motions from the step edge
(b) Particle motions from the bottom wall just downstream of the step

Fig. 12 Three-dimensional tracks of particle motion

suggests that the three-dimensionality of the flow is at least partly attributable to the existence of a corner vortex as pointed out by de Brederode and Bradshaw(1972).

The kinematic plausibility of the topological flow pattern illustrated in Fig. 13 may be checked by a topological rule. Kao et al.(1983) showed that the rule for skin friction lines on the interior

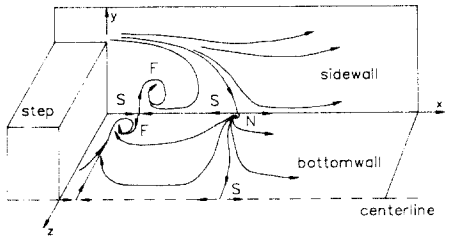

Fig. 13 Schematic diagram of surface flows

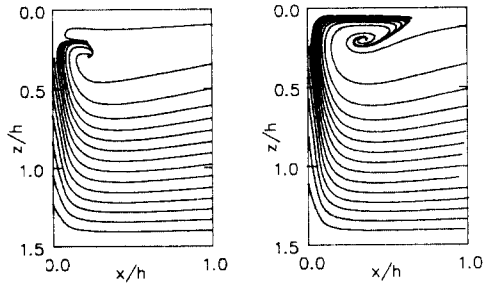

(a) $Re=1.0\times10^5$ (b) $Re=1.0\times10^4$

Fig. 14 Detailed description of surface flow pattern

surface of a one-fold torus (a geometry which is topologically equivalent to the present configuration) is given as

$$\Sigma_N+\Sigma_S=0, \tag{22}$$

where Σ_N denotes the sum of the indices for node points (including focus) and Σ_S the sum of the indices for saddle points. The index value for N is 1 and S is -1. Considering the symmetry of the flow, we have 6 nodes (4 foci and 2 nodes) and 6 saddle points (four along the sidewalls and two along the centerline). The summations of each index are $\Sigma_N=6$ and $\Sigma_S=-6$ so that Eq. (22) holds.

Figure 14 shows the variation of surface flow pattern near the step face with the Reynolds number. It is noted that the corner vortex moves closer to the step face as the Reynolds number increases. In laminar flow calculations, the corner vortex could not be identified. However, the shape of the limiting streamlines was similar to the case of turbulent flow. It might be guessed that the corner vortex appears only at high Reynolds numbers.

5. Conclusions

A three-dimensional backward-facing step flow in a square duct having the aspect ratio of three and undergoing two to three expansion was studied numerically. Additional caculation was also carried out for the flow of Stevenson et al.(1984) having the aspect ratio 1 and the expansion ratio 1:2. Predictions were compared with their experimental data. The following was found.

(1) The reattachment length for three-dimensional flow was much shorter than that for two-dimensional flow and varied across the duct width. This is thought to be due to the transport of momentum into the recirculation zone by the secondary motion represented as longitudinal vortices.

(2) In laminar flow, the reattachment length was strongly dependent on the Reynolds number as in two-dimensional flows. In turbulent three-dimensional flow, the effect of Reynolds number was significant when the aspect ratio was small as demonstrated from the predictions for the flow of Stevenson et al.

(3) In turbulent flow, the three-dimensionality could be characterized by the presence of the corner vortex. The location of the corner vortex was found to vary with the Reynolds number.

(4) The development of longitudinal vortices and topological flow pattern seemed to be more effectively described by the use of non-linear k-ε model.

(5) The longitudinal vortices evolved by the curvature of flow passage (pressure-driven) at the first stage. Later, it was influenced by the anisotropy of the turbulence.

Acknowledgements

The first author would like to express his sincere thanks to Prof. K. Kuwahara of ISASS, Japan for his interest about the work and com-

puter time made available to the first author during the initial stage of this research. He also would like to thank Dr. W.Y. Soh of NASA Lewis Research Center for making the Reference (Kao et al., 1983) available. Part of this research was supported by the Korea Science and Engineering Foundation.

References

Amano, R.S., 1984, "Develoment of a Turbulence Near-Wall Model and its Application to Separated and Reattached Flows," Numerical Heat Transfer, Vol. 7, pp. 59~75.

Armaly, B.G., Durst, F., Pereira, J.C.F. and Schonung, B., 1983, "Experimental and Theoretical Investigation of Backward-Facing Step Flow," J. Fluid Mech., Vol. 127, pp. 473~496.

Bradshaw, P., 1987, "Turbulent Secondary Flows," Ann. Rev. Fluid Mech., Vol. 19, pp. 53~74.

Chen, Y.S,. 1986, "A Computer Code for Three-Dimensional Incompressible Flows Using Nonorthogonal Body-Fitted Coordinate Systems," NASACR-178818.

de Brederode, V. and Bradshaw, P., 1972, "Three-Dimensional Flow in Normally Two-Dimensional Separation Bubbles : I. Flow Behind a Rearward-Facing Step," Aeronautical Report, No. 72-19, Imperial College.

Demuren, A.O. and Rodi, W., 1984, "Calculation of Turbulence-Driven Secondary Motion in Non-Circular Ducts," J.Fluid Mech., Vol. 140, pp. 189~222.

Denham, M.K. and Patrick, M.A., 1974, "Laminar Flow Over a Downstream Facing Step in a Two-Dimensional Flow Channel," Trans. Inst. Chem. Engrs., Vol. 52, pp. 361~367.

Di Prima, R.C. and Stuart, J.T., 1983, "Hydrodynamic Stability," J. Applied Mechanics, Vol. 50, pp. 983~991.

Durst, F. and Rastogi, A.K., 1979, "Theoretical and Experimental Investigations of Turbulent Flows with Separation," in "Turbulent Shear Flow," Durst, F., Launder, B.E., and Schmidt, F. W., Eds., Springer-Verlag, Newyork, Vol. 1, pp. 208~219.

Eaton, J.K., 1980, "Turbulent Flow Reattachment: An Experimental Study on the Flow and Structure behind a Backward-Facing Step," Ph.D Thesis, Stanford University.

Eaton, J.K. and Johnston. J.P, 1981, "A Review of Research on Subsonic Turbulent Flow Reattachment," AIAA. J., Vol. 19, pp. 1099~1100.

Gessner, F. B., 1982., "Corner Flow (Secondary Flow of the Second Kind)," The 1980-1981 AFOSR-HTTM-stanford Conferecnce on Complex Turbulent Flows, Stanford University, Vol. I., pp. 182~212.

Goldstein, R.J., Ericksen, V.L., Olson, R.M. and Eckert, E.R.G., 1970, "Laminar Separation, Reattachment and Transition of the Flow over a Downstream-Facing Step," Trans. ASME, J. of Basic Eng., Vol. 92, pp. 732~741.

Hackman, L.P., Raithby, G.D. and Strong, A. B., 1984, "Numerical Predictions of Flows Over Backward-Facing Steps," Int. J. Numer. Methods in Fluids, Vol. 4, pp. 711~724.

Humphrey, J.A.C., Whitelaw, J.H. and Yee, G., 1981, "Turbulent Flow in a Square Duct with Strong Curvature," J. Fluid Mech., Vol. 103, pp. 443~463.

Kao, H.C., Burstadt, P.L. and Johns, A.L., 1983, "Flow Visualization and Interpretation of Visualization Data for Deflected Thrust V/STOL Nozzles," NASA TM 83554.

Kim, J.J., 1987, "Investigation of Separation and Reattachment of a Turbulent Shear Layer: Flow Over a Backward Facing Step," Ph. D Thesis, Stanford University.

Launder, B.E. and Spalding, D.B., 1974, "The Numerical Calculation of Turbulent Flows," Comput. Methods in Applied Mech. and Engr., Vol. 3, pp. 269~289.

Lim, K.S., Park, S.O. and Shim, H.S., 1990, "A Low Aspect Ratio Backward-Facing Step Flow," Experimental Thermal and Fluid Science, Vol. 3, pp. 508~514.

Nallasamy, M., 1985, "Critical Evaluation of

Various Turbulence Models as Applied to Internal Fluid Flows," NASA TP 2474.

Patankar, S.V., 1980, Numerical Heat Transfer and Fluid Flow, McGraw-Hill

Qin, H., 1984, "Flow Characteristic of a Sudden Axisymmetric Expansion," PDR/CPDUIC/4, Imperial College of Science and Technology, London.

Rodi, W. et al., 1982, "The 1980-1981 AFOSR-HTTM-Stanford Conference on Complex Turbulent Flows," Stanford University, Vol. III., pp. 1495~1516.

Ruderich, R. and Fernholz, H.H., 1986, "An Experimental Investigation of a Turbulent Shear Flow with Separation, Reverse Flow, Reattachment," J.Fluid Mech., Vol. 163, pp. 283~322.

Spalding, D.B., 1972, "A Novel Finite Difference Formulation for Differential Expressions Involving both First and Second Derivatives," Int. J. Numer. Methods Engr. Vol. 4, pp. 551~556.

Speziale, C.G., 1987, "On Nonliner k-1 and k-ε Models of Turbulence," J.Fluid Mech., Vol. 178, pp. 459~475.

Stevenson, W.H., Thompson, H.D. and Craig, R.R.,1984, "Laser Velocimeter Measurements in Highly Turbulent Recirculating Flows," Trans. ASME, J. of Fluids Eng., Vol. 106, pp. 173~180.

Van Doormaal, J.P. and Raithby, G.D., 1984, "Enhancements of the Method for Predicting Incompressible Flows," Numerical Heat Transfer, Vol. 7, pp. 147~163.

White, F.M., 1974, "Viscous Fluid Flow," McGraw-Hill, pp. 123~125.